*Oxidation of Metals, Vol. 21, Nos. 3/4, 1984*

# Oxidation Behavior of 20% Cr/25% Ni/Nb Stabilized Stainless Steel in $CO_2$ Environments

**G. C. Allen,* P. A. Tempest,* J. W. Tyler,* and R. K. Wild***

*Received October 25, 1983; revised February 23, 1984*

*The oxidation of 20wt.% Cr/25wt.% Ni/Nb steel in 50 torr $CO_2$ at 1073 K has been studied "in situ" using X-ray photoelectron spectroscopy to determine the chemical composition of the oxide initially formed. The surface composition of the first formed oxide is shown to be iron rich, containing quantities of chromium and manganese, whilst analysis of the bulk oxide indicates that the majority of the oxide scale is a spinel of type $MnCr_{2-x}Fe_xO_4$. The formation of a chromia layer, which has been suggested to form first on these steels, was not observed. An examination of the oxide morphology using scanning electron microscopy revealed the presence of particle mounds varying in size from $<0.5\,\mu m$ to $\sim 3\,\mu m$ in diameter and embedded in the surface oxide. Other techniques, including scanning Auger microscopy and energy dispersive X-ray analysis, have been employed to determine the composition of these particles, and suggestions for their origin have been offered.*

**KEY WORDS:** stainless steel; high-temperature oxidation; X-ray photoelectron spectroscopy; scanning Auger microscopy.

## INTRODUCTION

Much of the early work on the oxidation of 20 wt.% Cr/25 wt.% Ni/Nb stabilized steel (20/25/Nb) in gaseous carbon dioxide was interpreted in terms of the initial rapid formation of a rhombohedral $Cr_2O_3$ layer followed by the development of a spinel type oxide at the gas/oxide interface formed by cationic diffusion.[1-3] More recently, the early stages of the growth of the surface oxide have been studied by a number of techniques for surface

*Central Electricity Generating Board, Berkeley Nuclear Laboratories, Berkeley, Gloucestershire, GL13 9PB, United Kingdom.

analysis including X-ray photoelectron spectroscopy (XPS), Auger electron spectroscopy (AES), X-ray fluorescence analysis (XRF), and X-ray diffractometry (XRD). We here report some of these investigations in which a sample of 20/25/Nb stabilized steel [a fuel cladding material used in the Central Electricity Generating Board's Advanced Gas Cooled Reactors (AGR)] of known thermal history has been oxidized under controlled conditions.

## EXPERIMENTAL PROCEDURE

A sample of as received 20/25/Nb stabilized steel (34 mm long, 11 mm wide, and 0.37 mm thick) was cut from a tube of AGR fuel can supplied by UKAEA Springfields in the form of single start ribbed pins of composition 19.7 wt.% Cr; 24.6 wt.% Ni; 0.6 wt.% Mn; 0.55 wt.% Si; 0.52 wt.% Nb; 0.03 wt.% C; balance Fe. The unannealed sample was flattened, mounted on a high temperature specimen probe, and inserted into a Kratos ES 300 electron spectrometer.[4] The surface was cleaned by 4 keV, 0.04 mA, argon ion bombardment for 4 hr and checked by recording a wide scan X-ray photoelectron spectrum monitoring the oxygen and carbon peaks. After heating the sample to 1073 K in the instrument's preparation chamber, research grade $CO_2$ (British Oxygen Company Ltd) was admitted at 50 torr for various periods of time. The foil was cooled in the ambient $CO_2$, which was subsequently removed by a combination of sorption pumps ($<1 \times 10^{-1}$ torr) and diffusion pumps ($<1 \times 10^{-7}$ torr) before the specimen was moved into the analysis chamber of the spectrometer. Wide scan XPS measurements were recorded using Al K$\alpha$ X-rays with the anode operated at 300 W and the source and collector slit widths set at 1.8 and 3.0 mm, respectively. The spectrometer was operated in the fixed analyzer transmission mode using a pass energy of 65 eV, and the binding energy scale was internally calibrated by use of the energy difference between Al K$\alpha$ and Mg K$\alpha$ radiation. The sample was oxidized in two stages for a total of 15 min, after which time it was removed from the spectrometer and examined using X-ray diffraction and reflectance spectroscopy.

X-ray diffraction patterns were recorded using a Philips PW 1050 vertical diffractometer, and reflectance spectra were obtained in the infrared, near infrared, and visible regions using Perkin-Elmer 180 and Beckman DK 2A spectrometers. The morphology and composition of the surface oxide was also examined using a Cambridge Stereoscan S150 scanning electron microscope (SEM) and a Physical Electronics 595 scanning Auger microprobe (SAM). The latter had a spatial resolution of $\sim$50 nm when used to obtain electron images and $\sim$100 nm when used for the analysis of Auger electrons from individual particles.

## RESULTS

### X-Ray Photoelectron Spectroscopy

The surface composition of the clean and oxidized foil was obtained from wide-scan X-ray photoelectron spectra by measuring the height of the recorded peak above the background and correcting for the relative yield of the element using the sensitivity factors of Wagner *et al.*[5] The results expressed as atom percent are summarized in Table I. For the unoxidized metal, the bulk and surface composition is somewhat similar, but on oxidation the surface composition changes dramatically. After oxidation for only 5 min, nickel was no longer detected at the surface (and remained absent for the remainder of the oxidation period), but manganese occurred in the surface oxide. In addition the level of chromium was observed to decrease steadily as oxidation proceeded until, after 15 min, the metal composition of the surface was 17.1 at.% iron, only 5.3 at.% chromium, but 1.8 at.% manganese.

Binding energies of the $2p_{1/2,3/2}$ photoelectron peaks recorded for chromium, iron, and nickel from the clean metal surface were, as expected, representative of those recorded from the pure metals.[6–8] On oxidation the Cr $2p$ photoelectron spectrum was shifted to higher binding energies and was characteristic of that from the $Cr^{3+}$ ion in an octahedrally coordinated oxide environment.[6] The Fe $2p$ photoelectron peaks also exhibited a structure characteristic of the $Fe^{3+}$ ion after oxidation for 5 min, but further oxidation produced a profile which indicated the presence of $Fe^{2+}$ also.[7]

**Table I.** Surface Composition (at.%) of 20 wt.% Cr/25 wt.% Ni/Nb Steel after Oxidation for 15 Minutes in 50 torr $CO_2$ at 1073 K Determined Using X-ray Photoelectron Spectroscopy

| | Surface composition (at.%) at oxidation time of | | | |
|---|---|---|---|---|
| Element | 0 min | 5 min | 15 min | Bulk composition (at.%) |
| Cr | 17.1 | 9.4 | 5.3 | 22.0 |
| Ni | 14.5 | 0.0 | 0.0 | 24.1 |
| Fe | 56.0 | 12.1 | 17.1 | 53.0 |
| Mn | 0.0 | 4.6 | 1.8 | 0.6 |
| Nb | 0.0 | 0.0 | 0.0 | 0.3 |
| O | 8.6 | 73.9 | 75.8 | 0.0 |
| C | 3.8 | 0.0 | 0.0 | 0.0 |

For manganese the Mn $2p$ signal was rather weak, and it was not possible to unambiguously identify the oxidation state of this element in the oxide film.

## X-Ray Diffraction and Oxide Thickness

On completion of oxidation in the X-ray photoelectron spectrometer, the sample was removed and the total oxide thickness determined using two independent techniques: X-ray diffraction and visible/ultraviolet diffuse reflectance electronic absorption spectroscopy. Analysis of the X-ray diffraction pattern showed that the oxide scale was composed of a cubic spinel phase of lattice parameter $8.47 \pm 0.02$ Å, a rhombohedral $Cr_2O_3$ phase, and a third cubic phase corresponding to NbC. A quantitative analysis of the most intense spinel and rhombohedral diffraction peaks, by the method described by Tempest and Wild,[9] determined the total thickness of the oxide layer to be $0.03(4) \pm 0.02$ $\mu$m, the thickness ratio of the spinel and rhombohedral layers being 3 : 1.

The thickness of the thin oxide film was also determined by analysis of the separation between the interference fringes observed in the UV/visible diffuse reflectance spectrum.[10] Such fringes are observed when the thickness of the oxide layer is of the same order of magnitude as the wavelength of the incident radiation, and they are formed by interference between radiation reflected from the air/oxide interface and that reflected from the oxide/metal interface. Analysis by this method gave a total oxide thickness of $0.09 \pm 0.08$ $\mu$m.

## Oxide Morphology

Scanning electron micrographs of a representative area of the oxidized sample are shown in Fig. 1. The surface consisted of a thin, uniform, and compact oxide layer littered with a variety of irregularly shaped particles, together with a few more rounded particles. Although the majority of these particles were $<0.5$ $\mu$m in size, a few larger ones were $\sim 3$ $\mu$m in diameter. Individual particles appeared split by convoluted fissures but were otherwise devoid of distinctive surface features.

## Energy Dispersive X-Ray Analysis (EDX)

Spot analysis from various particles and the background oxide illustrated in Fig. 1 was carried out by energy dispersive X-ray analysis. To reduce the signal from the underlying substrate and to determine qualitatively the elemental composition as a function of depth, the analyses were carried out using 10 and 20 kV beam voltages. The K$\alpha$ lines from the

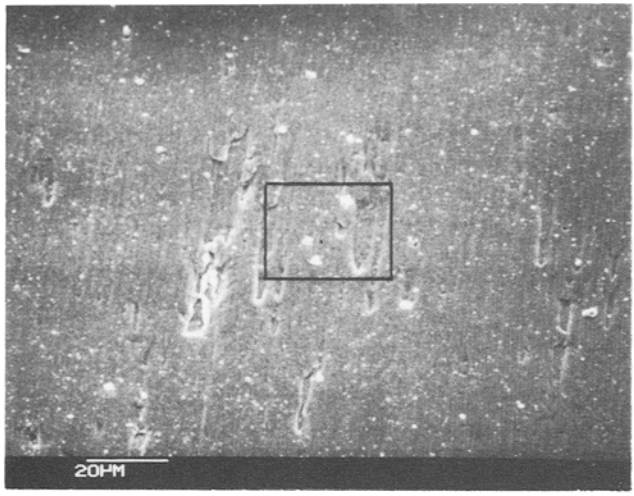


(a) LOW MAG. VIEW OF SURFACE

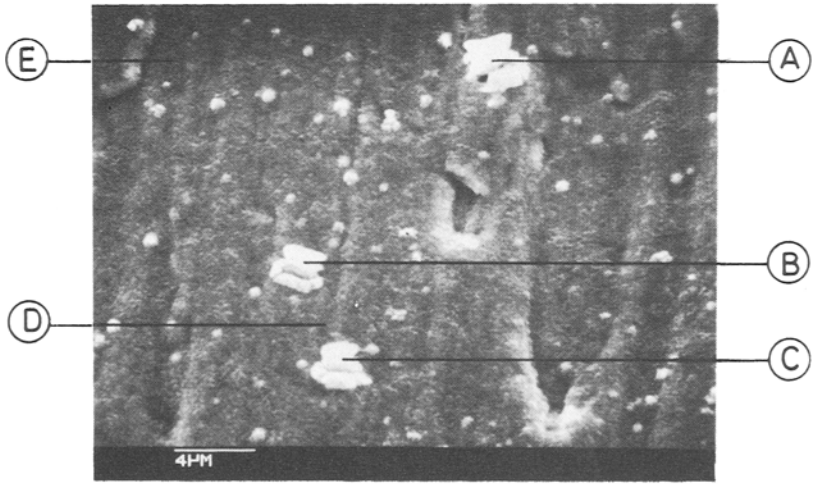


(b) HIGH MAG. VIEW OF BOXED AREA

**Fig. 1.** Scanning electron micrographs of 20 wt.% Cr/25 wt.% Ni/Nb stabilized steel oxidized in 50 torr $CO_2$ at 1073 K for 15 min.

elements present were counted for 100 s and the appropriate background correction and sensitivity factors taken into account. The results are displayed as metal ratios in Table II.

The particles were evidently rich in niobium, but the analyses at 10 and 20 kV shows significant differences. At 10 kV the particles analyzed contained mainly niobium, but the other constituents were mostly iron and chromium with traces of nickel, manganese, and silicon present. The 20 kV analyses showed a wider diversity with increased iron, chromium, and nickel contents clearly indicating the presence of the substrate metal in the volume analyzed. This effect was also seen in the analysis of the background oxide, where the penetration of the electron beam was greater than the oxide thickness in both cases (penetration of a 10 keV electron beam into chromium is estimated at ~0.2 $\mu$m). In fact, at 20 kV the composition determined for the background oxide approximated fairly closely to the composition of the bulk metal (see Table I). On the other hand, the analysis at 10 kV indicated an enrichment of chromium and iron relative to nickel in the oxide scale in accord with the lattice parameter measurement from the X-ray diffraction analysis.

## Replication

An attempt was made to remove the uncertainty regarding the contribution to the X-ray signal from the substrate metal by stripping particles from

**Table II.** Energy Dispersive X-Ray Analysis of Particles and Background Oxide on 20 wt.% Cr/25 wt.% Ni/Nb Stabilized Steel Oxidized for 15 Minutes in 50 torr $CO_2$ at 1073 K

| | | Metal ratio for particle | | | Background oxide | |
|---|---|---|---|---|---|---|
| kV | Element | A | B | C | D | E |
| 20 | Si | 0.3 | 0.1 | 0.2 | 0.3 | 0.4 |
| | Nb | 45.8 | 50.3 | 31.8 | 1.0 | 0.5 |
| | Cr | 14.5 | 13.9 | 17.8 | 24.3 | 22.7 |
| | Mn | 0.4 | 0.1 | 0.3 | 0.0 | 0.4 |
| | Fe | 29.2 | 26.3 | 36.6 | 54.2 | 55.1 |
| | Ni | 9.8 | 9.3 | 13.3 | 20.2 | 20.9 |
| 10 | Si | 0.1 | 0.1 | 0.0 | 0.9 | 0.7 |
| | Nb | 84.2 | 91.5 | 77.6 | 1.5 | 0.9 |
| | Cr | 4.1 | 4.5 | 13.1 | 29.8 | 34.0 |
| | Mn | 0.3 | 0.0 | 0.0 | 1.6 | 1.6 |
| | Fe | 6.8 | 3.9 | 8.9 | 51.6 | 51.2 |
| | Ni | 4.5 | 0.0 | 0.4 | 14.6 | 11.6 |

the oxide surface using replication. Carbon replicas were produced from a small section of the sample following the procedure outlined by Betteridge and Heslop.[11] On examination in the SEM, a variety of rounded featureless particles were observed embedded in the carbon film, ranging in size from $<1/2\ \mu$m to $>2\ \mu$m. EDX again showed the particles to be niobium rich. Some were composed almost entirely of niobium with only traces (1–2%) of chromium, iron, and silicon present. Others gave metal ratios similar to those presented in Table II, whilst a few displayed relatively large concentrations of chromium and manganese. In the majority of cases nickel was not observed, but was present in trace amounts ($\sim$1%) in some particles. The absence of this element suggested that the contribution from the metal substrate was very small in the analyses at 10 kV. It is, however, puzzling that an increased diversity in the metal ratios was observed in the replicated particles compared with the "in situ" analysis. It is possible that either different quantities of oxide scale were removed with the particles on replication or the etching process had altered the chemical composition of the extracted particles (as indicated by the loss of surface detail).

## Scanning Auger Microscopy

Figures 2(a–c) show scanning electron micrographs recorded in the scanning Auger microprobe. As discussed above, two types of particle could be identified at the surface of the oxide. The first and most common type was that with deep fissures, illustrated in Fig. 2(c). The second type, often spherical in shape, had a much smoother surface, as indicated in Fig. 2(b).

Point analysis of both the surface oxide and the two particle types was carried out, and representative Auger spectra are reproduced in Fig. 2. The background oxide (area A, Fig. 2b) was found to be iron rich, containing approximately 20% chromium. Analysis of the smooth particles indicated a composition rich in both aluminum and oxygen, with the elements calcium, chromium, iron, and silicon also present. In contrast, the irregularly shaped fissured particles showed high niobium levels, but also incorporated chromium, iron, and occasionally manganese. The surface of these particles and the background oxide was covered with a thin layer of amorphous carbon which, together with 10–15 nm of surface material, was removed by a short period of argon ion sputtering. The background oxide then appeared carbon free and the carbon Auger line, recorded at 263 eV from the irregularly shaped particles, was entirely characteristic of a carbide species.

In Figs. 3 and 4 the carbon regions of the Auger spectrum have been expanded to show the shape of the peaks. A number of Auger profiles for carbon have been reported,[12] and reference to these identified the bulk material as niobium or chromium carbide. Data from the surface oxide and

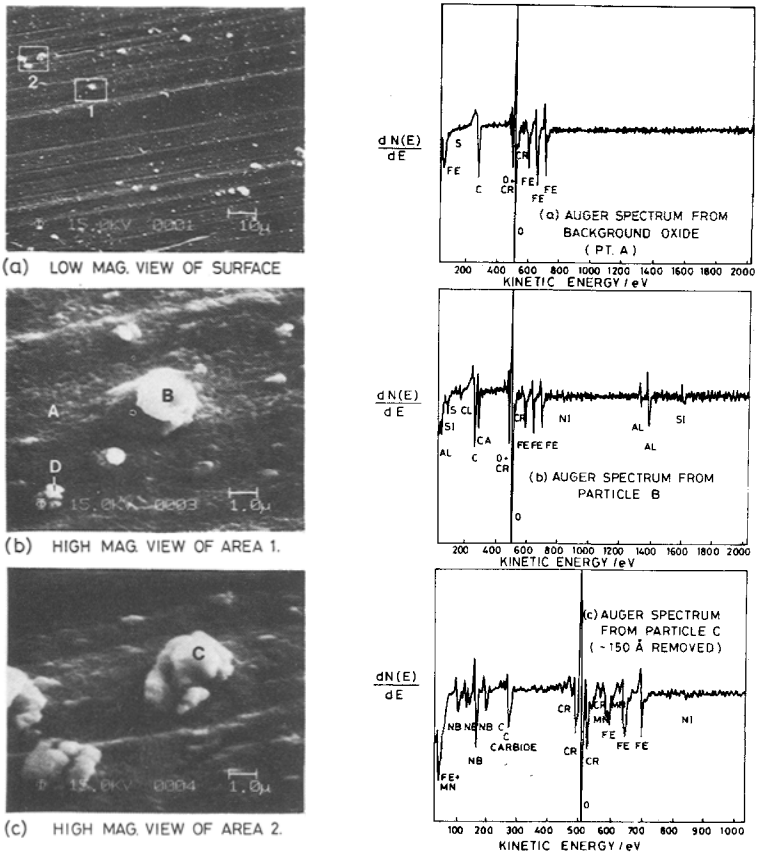


**Fig. 2.** Electron micrographs and Auger spectra of the surface of 20 wt.% Cr/25 wt.% Ni/Nb stabilized steel oxidized in 50 torr $CO_2$ at 1073 K for 15 min.

various embedded particles, summarized in Table III, indicated that the particles were made up of both oxide and carbide. By assuming that the oxide present was of type $M_2O_3$, metal/carbon ratios were estimated at 6.6/1 for the particle at point D in Fig. 2(b) and 2.86/1 for the particle at point C in Fig. 2(c). Thus carbides of approximate composition $M_6C$ and $M_3C$ or $M_7C_3$, respectively, were indicated. On the other hand, if it was assumed that all the carbon was in the form NbC then, in each case, the amount of oxygen detected was insufficient to form an oxide without the presence of free metal at the surface of the particle. It is possible that bombardment of the particle with argon ions reduced the oxide at the surface, leading to a lower than expected oxygen concentration. Alternatively, the formation of a carbide of type $M_{23}C_6$ would leave insufficient

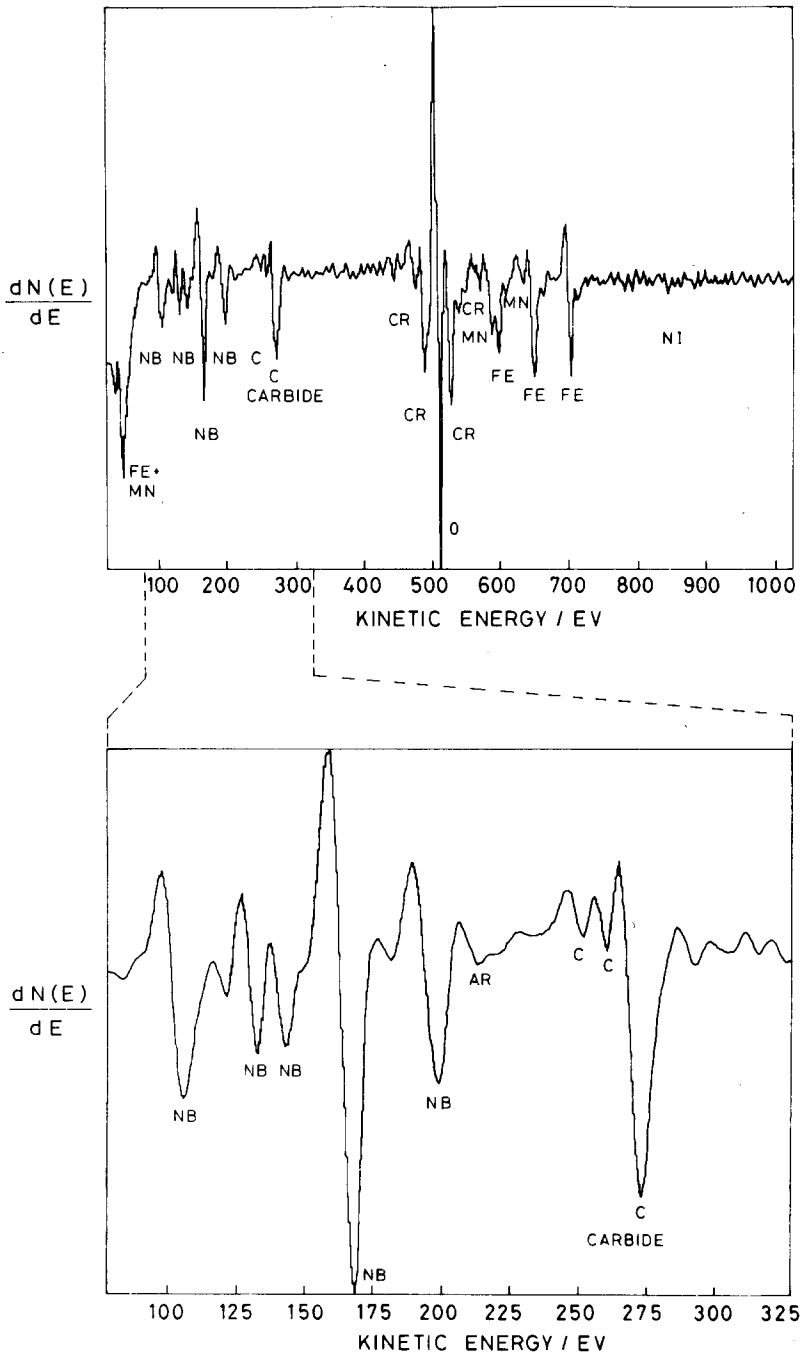


**Fig. 3.** Auger spectrum of particle (point C, Fig. 2c, ~15 nm removed) on the surface of 20 wt.% Cr/25 wt.% Ni/Nb stabilized steel oxidized in 50 torr $CO_2$ at 1073 K for 15 min with the carbon region expanded to show the characteristic carbide peak shape.

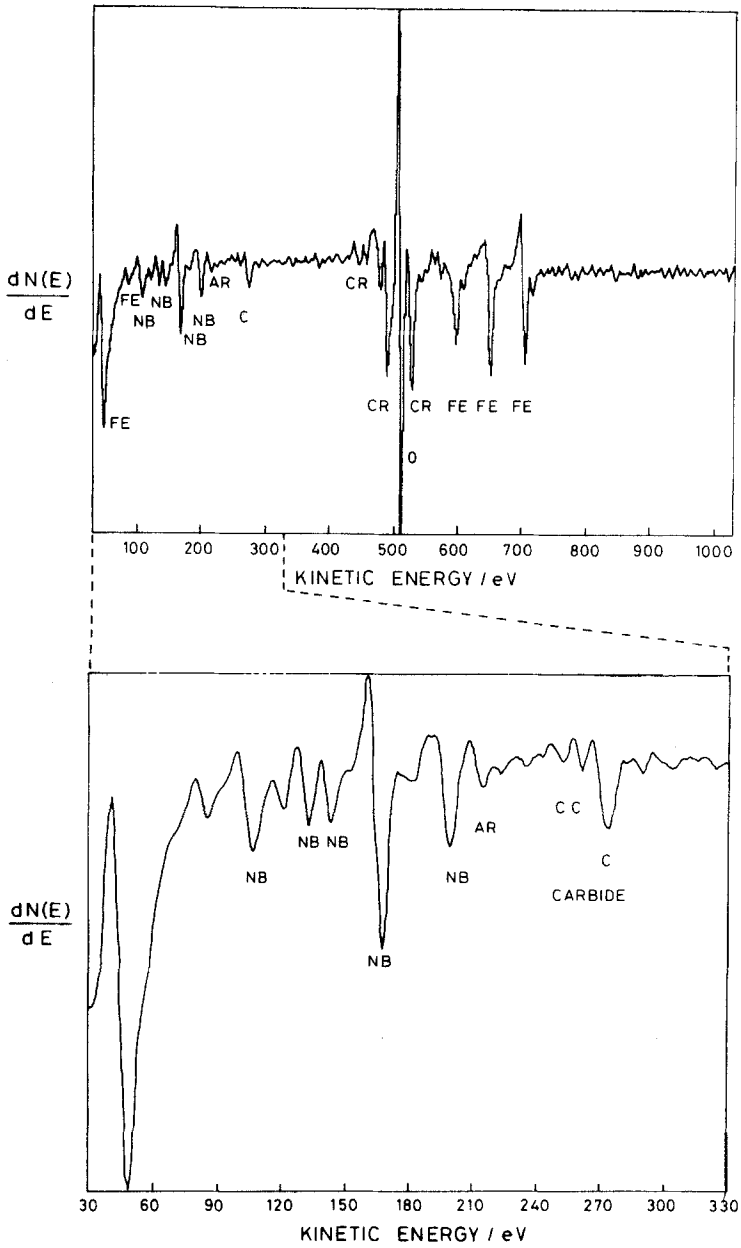


**Fig. 4.** Auger spectrum of particle (point D, Fig. 2b, ~10 nm removed) on the surface of 20 wt.% Cr/25 wt.% Ni/Nb stabilized steel oxidized in 50 torr $CO_2$ at 1073 K for 15 min with the carbon region expanded to show the characteristic carbide peak shape.

**Table III.** Surface Composition of Particles and Oxide on 20 wt.% Cr/25 wt.% Ni/Nb Stabilized Steel Oxidized for 15 Minutes in 50 torr $CO_2$ at 1073 K as Determined by Scanning Auger Microscopy

| | Composition (at.%) | | | |
|---|---|---|---|---|
| | Background oxide | Regular particle | Carbide particle 1 (*PtD* in Fig. 2b) | Carbide particle 2 (*PtC* in Fig. 2c) |
| Element | Before sputtering | | After sputtering | |
| C | 40.1 | 24.0 | 8.6 | 19.4 |
| O | 20.4 | 14.4 | 20.7 | 15.1 |
| Si | | 1.9 | | |
| Al | | 37.7 | | |
| Ca | | 5.0 | | |
| Cr | 8.6 | 4.2 | 25.0 | 18.0 |
| Mn | | | | 8.5 |
| Fe | 30.2 | 12.3 | 30.1 | 19.1 |
| Nb | | | 15.6 | 19.9 |

metal to form an oxide in particle D, Fig. 2(b), but would indicate the presence of an $MO_2$ type oxide in the particle at point C in Fig. 2(c).

The accuracy of the above quantitative analysis was dependent upon the complexity of the system studied and the availability of well-characterized standards. The values quoted in Table III are accurate to within ±5–10 at.%,[13] which was sufficient to indicate differences and trends between the M:O and M:C ratios of different oxide/carbide particles.

## DISCUSSION

### Nature of the Oxide First Formed on 20/25/Nb Steel

The excellent corrosion resistance of 20/25/Nb steel in $CO_2$ environments is attributed to the formation of a dense chromium rich oxide layer, which acts as a protective barrier between the bulk metal and the corrosive gas phase.[14] Further oxidation is inhibited by slowing the outward diffusion of metal cations.

Much of the previous work on 20/25/Nb has been concerned with oxidation kinetics (particularly long term weight gain measurements) and characterization of the scale morphology and composition using SEM, EDX, and EPMA. Usually the oxide scale has been studied only after

relatively long oxidation times, $\gg$100 hr, when the several micron thickness of the oxide layer is sufficient for accurate analysis. EPMA has shown that the oxide formed on this steel following thousands of hours oxidation in $CO_2$ at 1023–1173 K is duplex in nature, consisting of an outer iron-rich spinel containing manganese and chromium covering an inner rhombohedral chromium rich layer and a thin silica layer which forms at the metal/oxide interface.[1–3,9,15–20] The early data were generally interpreted in terms of the initial formation of a protective $Cr_2O_3$ layer through which the spinel layer grows by cationic diffusion.

More recently, the composition of the surface oxide formed on 20/25/Nb after short periods of time (1 min–100 hr) has been investigated "in situ" using the surface sensitive techniques of AES[21] and XPS.[22] Tempest and Wild[21] have observed only iron oxide on the surface of a sample oxidized for 1 min in 1 atm $CO_2$ at 1123 K. On further oxidation they noted the incorporation of nickel, manganese, and chromium into the iron oxide surface and showed that after 100 hr oxidation, the bulk of the oxide present had a spinel structure, although a rhombohedral phase amounting to about 10% of the total oxide was also detected. Similar results have been observed by Tyler[22] for a sample oxidized in 50 torr $CO_2$ at 973 K for 2 min–100 hr. In contrast, for samples oxidized at 1123 K in $7\times10^{-3}$ torr $CO_2$ for 20 hr, a chromia layer was formed, the partial pressure of $CO_2$ being sufficiently low to prevent significant oxidation of the iron and nickel components in the steel surface.

In the present work, at the commencement of oxidation there was no indication of the formation of a chromia layer at the alloy surface. Rather, the oxide produced after exposure of the metal at 1073 K to 50 torr $CO_2$ for 15 min was shown by XPS to be enriched in iron and to contain quantities of chromium and manganese, a result which agreed with the SAM analysis (see Tables I and III). The bulk oxide analyses accorded with the observed surface compositions. XRD showed that the majority of the oxide present after 15 min oxidation was a spinel of lattice parameter $8.47 \pm 0.02$ Å. Earlier, Tempest and Wild[20] pointed out that the most probable spinel with lattice parameters between 8.44 Å ($MnCr_2O_4$) and 8.51 Å ($MnFe_2O_4$) took the form $MnCr_{2-x}Fe_xO_4$ and noted that while Vegard's law is not strictly obeyed for solid solutions of the type $MnCr_{2-x}Fe_xO_4$, a lattice parameter of 8.47 Å indicated a spinel containing approximately equal concentrations of iron and chromium. While the overall mechanism of duplex oxide growth on 20/25/Nb steel is still somewhat uncertain, it seems clear that the nature of the oxides formed initially is sensitive to the oxidation temperature and pressure and that kinetic rather than thermodynamic factors govern the initial oxide growth.

## Origin and Analysis of the Carbide/Oxide Mounds

In order to prevent the sensitization of fuel cladding on prolonged exposures to temperatures in the region 773–1123 K, niobium is added to 20/25 steel to act as a stabilizer. The cladding possesses a stable grain size of ~25 $\mu$m with a random dispersion of Nb(C, N) precipitates ranging in size from <0.1 to ~3.0 $\mu$m. Whilst it is difficult to measure accurately the surface area fraction of the precipitates exposed to the oxidizing atmosphere, backscattered electron images in the SEM indicated that the concentration of precipitates a the surface was similar to the bulk volume fraction.

Secondary electron images of the unoxidized sample displayed a uniform, relatively smooth surface marked by microscratches and pits caused by machining. However, after oxidation for only 15 min, the morphology of the metal surface was observed to undergo a dramatic change, displaying particles or mounds of carbide/oxide in a wide variety of sizes (Figs. 1 and 2). Extended ridges of the carbide/oxide were not observed, however, which suggested that the mounds were formed at distinct sites rather than by selective oxidation at grain boundaries. Niobium carbide was the only carbide phase detected by X-ray diffraction after oxidation, whereas the Auger results from individual particles indicated the presence of carbide and oxide species in varying proportions. Energy dispersive X-ray analysis of the metallic elements, on the other hand, showed the particles to contain up to 90% niobium with smaller amounts of iron and chromium also present. We conclude, therefore, that the niobium carbide precipitates present at the surface of the metal are oxidized/coarsened on exposure to the $CO_2$ environment and that individual precipitates at the surface act as separate centers to provide the observed distribution of particle sizes.

It is not easy to predict the ultimate product of such coarsening/oxidation processes when the carbon activity at the scale/gas interface is uncertain. In the present experiment the carbon activity could not be ascertained unambiguously because of the wide range of reactions which could occur between the gas and solid phases in the enclosed system. Each reaction would change the thermodynamic equilibrium as oxidation proceeded. However, an indication was provided by considering the precipitation behavior of different carbides in 20/25/Nb steels. Knowles[23] has pointed out that a prediction of the types of precipitate likely to occur may be made by considering the degree to which matrix chromium is stabilized by the addition of niobium. This degree of stabilization is expressed as wt.% Nb/wt.% (C+N), and these predictions are reproduced in Table IV. Thus chromium bearing $M_{23}C_6$ would not be expected to be precipitated when enough niobium is retained in solution to form stoichiometric NbC

**Table IV.** Precipitation in 20 wt.% Cr/25 wt.% Ni/Nb Steels[a]

| Ratio of Nb/(C+N) | Predicted equilibrium phase |
|---|---|
| 0 | $M_{23}C_6$ |
| <7.7 | $NbC + M_{23}C_6$ |
| >7.7 | $NbC + M_6C$ |
| >23.1 | $M_6C$ + niobides |

[a]Data from Knowles.[23]

(Nb/(C+N) ratio of ~7.7). Similarly the carbide $M_6C$ (as $Nb_3M_3C$) will be the favored precipitate for Nb/(C+N) ratios between 7.7 and 23.1. Control of the Nb/(C+N) ratio in the steel (as noted above) thus influences the ultimate type of carbide dispersion produced. Knowles notes that the predictions are necessarily approximate since no account is taken of nucleation conditions or the solubility and segregation of solute atoms, but that reasonable agreement is found with observations reported in the literature.

The steel used here possesses a Nb/(C+N) ratio of ~17.3. Thus any NbC precipitated would be expected to coarsen progressively on ageing and transform to $M_6C$. (From the thermodynamic considerations the carbide $M_{23}C_6$ would not be expected to form.) Several authors[24,25] have in fact noted this transition in Nb stabilized steels possessing similar Nb/C+N ratios. Dewey *et al.*[24] observed the intergranular and grain boundary precipitation of NbC in cold worked unannealed 20/25/Nb, which subsequently coarsened and transformed to $M_6C$ on ageing at 923 K in vacuum for periods up to 5000 hr. Sumerling and Nutting[25] observed the formation of sigma particles together with dendritic $M_6C$ carbides at grain boundaries in a steel aged for 5000 hr at 973 K. By analogy we might then predict that the NbC precipitates present at the surface of the steel would, on exposure to an oxidizing environment at 1073 K, begin to oxidize and incorporate matrix cations to form eventually a mixture of oxide and $M_6C$.

Before a mechanism for the particle formation is proposed, it is important to consider the information obtained by the different spectroscopic techniques used. The Cu K$\alpha$ X-rays used in the X-ray diffraction experiment penetrate the steel to a depth of ~10 $\mu$m, so the information obtained is derived from a similar depth. The region sampled therefore included the matrix austenitic phase, the surface oxide, the primary NbC precipitates, and coarsened precipitates (if present in sufficient quantity). X-rays excited by a 20 keV electron beam originate from an "onion" shaped volume ~2–3 $\mu$m in depth, while backscattered electrons produced with the same

beam energy emanate from $\sim 1\ \mu m$. Secondary electrons are generated within $\sim 50\ \mu m$ of the surface, but Auger electron spectroscopy samples only a few atom layers. Thus the Auger spectrum may be considered to represent the surface of a carbide/oxide particle while EDX analysis incorporates the carbide/oxide mound, together with any original NbC precipitate and probably a contribution from the underlying matrix steel. The high proportion of Nb detected in the particle by EDX could thus be interpreted in terms of an underlying NbC precipitate of which the majority has yet to coarsen or react.

The surface of the smaller of the two particles analyzed by SAM was shown to be $M_6C$, assuming effects from $Ar^+$ bombardment were absent and that all the oxygen detected was present as an $M_2O_3$ type oxide. By assuming that all the Nb detected was associated with the carbide, its composition may be written as $Nb_2M_4C$, where M = Fe or Cr. The ratio of iron to chromium in the carbide cannot be directly inferred without assuming the composition of the associated oxide. However, if the chromium and iron levels in the oxide are comparable then a similar situation will exist for the carbide. No manganese or nickel was detected in the particle. This composition lies within the range of stoichiometries observed by Kuo,[26] who showed that the composition of $M_6C$ can vary between $Nb_2M_4C$ and $Nb_3M_3C$ (M = Fe, Cr, Ni). Observations at longer oxidation times (100 hr) but at lower temperatures (973 K) have identified $Nb_3M_3C$ in the surface region.[22]

The composition of the $M_6C$ carbide is of interest because of the possibility of sensitization of the matrix steel when aged in the temperature range 693–823 K. Sensitization of the fuel cladding alloy could be caused by chromium depleted zones adjacent to the $M_6C$ carbides at grain boundaries. The presence of such zones has been reported by Pande *et al.*[27] to surround $M_{23}C_6$ carbides in type 304 (19% Cr/8% Ni) stainless steel. To date no such evidence for this effect has been reported for 20/25/Nb stabilized steel, possibly because such zones are too narrow to be detected with electron beams of diameter > 25 cm, but Čihal and Ježek[28] have observed in 18/12/Nb steel that $M_6C$ is enriched in chromium at an ageing temperature of 923 K, although $Fe_3Nb_3C$ phases were observed at higher temperatures. Curiously, however, Ransetta and Scott[29] found $M_6C$ formed in a 20/25/Nb steel aged for 3000 hr at 923 K to be more consistent with the general formula $[Ni + (Fe + Cr)]_3Nb_3(C, N)$, which is nickel rich, containing only small quantities of iron and chromium. Although the composition of the carbide/oxide mounds reported here may not be directly comparable with the coarsened NbC precipitates observed in aged steels in view of the involvement of an oxidizing species and the likelihood that the particles are still in the process of coarsening or oxidizing, the scanning Auger results

nevertheless indicate that equal concentrations of iron and chromium are present in the carbide component of the particles, reflecting the slightly higher diffusion rate of chromium compared with the other major elements present.

The formation of particles during oxidation of the metal surface may therefore be regarded as follows:

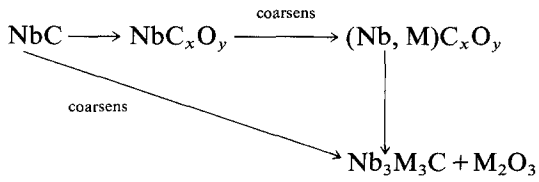


where M = Fe, Cr, Ni.

## CONCLUSIONS

First, we have shown that the surface composition of the oxide which forms on 20/25/Nb stainless steel when oxidized for 15 min in 50 torr $CO_2$ at 1073 K is iron rich, containing quantities of chromium and manganese, while analysis of the bulk oxide shows that the majority of the oxide scale is an $MnCr_{2-x}Fe_xO_4$ type spinel. The formation of an initial chromia layer, which has been suggested to form first on these steels, was not observed. Second, the particle mounds varying in size from $<0.5$ to $\sim 3$ $\mu$m in diameter observed embedded in the surface oxide were shown to be comprised of a mixture of carbide and oxide. Their presence is attributed to the coarsening/oxidation of matrix NbC precipitates present at the gas/metal interface. It is suggested that these mounds are in the process of coarsening to an $M_3Nb_3C$ carbide containing approximately equal concentrations of chromium and iron.

## ACKNOWLEDGMENT

This paper is published by permission of the Central Electricity Generating Board.

## REFERENCES

1. J. M. Francis and W. H. Whitlow, *J. Iron and Steel Inst.* **203**, 468 (1965).
2. J. M. Francis, *Br. Corr. J.* **3**, 113 (1968).
3. J. M. Francis, C. J. Lee, and J. H. Buddery, *J. Iron Steel Inst.* **206**, 921 (1968).
4. G. C. Allen, P. M. Tucker, and R. K. Wild, *Surface Sci.* **68**, 469 (1977).
5. C. D. Wagner, L. E. Davis, M. V. Zeller, J. A. Taylor, R. H. Raymond, and L. H. Gale, *Surface Interface Anal.* **3**, 211 (1981).

6. G. C. Allen, P. M. Tucker, and R. K. Wild, *J. Chem. Soc. Faraday Trans. II* **74**, 1126 (1978).
7. G. C. Allen, P. M. Tucker, and R. K. Wild, *Phil. Mag. B* **46**, 411 (1982).
8. G. C. Allen, P. M. Tucker, and R. K. Wild, *Oxid. Met.* **13**, 223 (1979).
9. P. A. Tempest and R. K. Wild, *Oxid. Met.* **17**, 345 (1982).
10. G. C. Allen and G. A. Swallow, *Oxid. Met.* **17**, 141 (1982).
11. W. Betteridge and J. Heslop, *The Nimonic Alloys*, 2nd ed. (Edward Arnold, London, 1974), p. 69.
12. C. C. Chang, *Characterisation of Solid Surfaces* (Plenum Press, New York, 1974), p. 509.
13. R. K. Wild, *Vacuum* **31**, 183 (1981).
14. R. L. Cowan and C. S. Tedman, Jr., in *Advances in Corrosion Science and Technology*, M. G. Fontana and R. W. Staehle, eds. (Plenum Press, New York, 1973), Vol. 3, p. 293.
15. J. M. Francis, M. T. Curtis, and D. A. Hilton, *J. Nucl. Mat.* **41**, 203 (1971).
16. H. E. Evans, R. Hales, D. A. Hilton, R. A. Holm, G. Knowles, and R. J. Pearce, *BNES Conf. Corr. of Steels in $CO_2$ Reading* (1974), p. 284.
17. H. E. Evans, D. A. Hilton, and R. A. Holm, *Oxid. Met.* **10**, 149 (1976).
18. H. E. Evans, D. A. Hilton, R. A. Holm, and S. J. Webster, *Oxid. Met.* **14**, 235 (1980).
19. P. Skeldon, J. M. Calvert, and D. G. Lees, *Proc. Roy. Soc.* **A292**, 545 (1980).
20. P. A. Tempest and R. K. Wild, *J. Nucl. Mat.* **102**, 183 (1981).
21. P. A. Tempest and R. K. Wild, CEGB Report RD/B/5179N81 (1981).
22. J. W. Tyler, unpublished results.
23. G. Knowles, CEGB Report RD/B/M2419 (1973).
24. M. A. P. Dewey, G. Sumner, and I. S. Brammar, *J. Iron Steel Inst.* **203**, 938 (1965).
25. R. Sumerling and J. Nutting, *J. Iron Steel Inst.* **203**, 398 (1965).
26. K. Kuo, *Acta Met.* **1**, 301 (1953).
27. C. S. Pande, M. Suenaga, B. Vyas, H. S. Isaacs, and D. F. Harling, *Scripta Met.* **11**, 681 (1977).
28. V. Čihal and J. Ježek, *J. Iron Steel Inst.* **202**, 124 (1964).
29. G. V. T. Ranzetta and V. D. Scott, *Met. Mat.* 146 (1967).